aerospace

MDPI

Article

Characterization and Testing of the Passive Magnetic Attitude Control System for the 3U AstroBio CubeSat

Stefano Carletta [1,*], Augusto Nascetti [1], Sagar S. Gosikere Matadha [1], Lorenzo Iannascoli [1], Thiago Baratto de Albuquerque [1], Nithin Maipan Davis [1], Luigi Schirone [1], Gabriele Impresario [2], Simone Pirrotta [2] and John R. Brucato [3]

[1] School of Aerospace Engineering, Sapienza University of Rome, Via Salaria 851, 00138 Rome, Italy
[2] Italian Space Agency, Via del Politecnico snc, 00133 Rome, Italy
[3] National Institute for Astrophysics, Arcetri Astrophysical Observatory, Largo Enrico Fermi 5, 50125 Florence, Italy
* Correspondence: stefano.carletta@uniroma1.it

Abstract: AstroBio CubeSat is a mission funded by the Italian Space Agency aimed at validating novel lab-on-chip technology, that would enable the use of micro- and nanosatellites as autonomous orbiting laboratories for research in astrobiology. This 3U CubeSat is equipped with a passive magnetic attitude control system (PMACS), including permanent magnets and hysteresis strips, which allows for stabilizing the spacecraft with the longitudinal axis in the direction of the geomagnetic field vector. This work presents the process followed for the experimental characterization of the system, performed on the engineering unit of the satellite by using a Helmholtz cage facility and a spherical air-bearing to recreate environmental conditions similar to the ones experienced during the orbital motion. The hysteresis strips are characterized starting from the determination of the hysteresis loop, from which the energy dissipation per cycle and the apparent magnetic permeability are extracted. Tests performed by using the Helmholtz cage and the air-bearing facility allows for further investigating the damping torque produced by the PMACS and validating the abovementioned parameters. Numerical analysis is then used to select the number of permanent magnets which allows for achieving a pointing accuracy within an error of 10° within 24 h from the deployment. The analysis of the flight data supports the results obtained from the experimental test campaigns, confirming the effectiveness of the proposed methods and of the PMACS design.

Keywords: AstroBio CubeSat; passive magnetic attitude control; Helmholtz cage; ADCS; experimental testing

Citation: Carletta, S.; Nascetti, A.; Gosikere Matadha, S.S.; Iannascoli, L.; Baratto de Albuquerque, T.; Maipan Davis, N.; Schirone, L.; Impresario, G.; Pirrotta, S.; Brucato, J.R. Characterization and Testing of the Passive Magnetic Attitude Control System for the 3U AstroBio CubeSat. *Aerospace* **2022**, *9*, 723. https://doi.org/10.3390/aerospace9110723

Academic Editors: Mikhail Ovchinnikov and Paolo Tortora

Received: 1 August 2022
Accepted: 2 November 2022
Published: 17 November 2022

1. Introduction

AstroBio CubeSat (ABCS) was a mission funded by the Italian Space Agency (ASI) aimed at validating the use of nanosatellites, developed by using the CubeSat standard, to perform autonomous research in astrobiology. The scope of the 3U ABCS was to validate a novel lab-on-chip technology to perform bio-analytical experiments in space and allow autonomous biological detection, based on chemiluminescence [1–3].

ABCS was launched on 13 July 2022 from Guiana Space Centre as a secondary payload of the Vega-C maiden flight and was deployed by the Vega-C along a circular orbit with altitude of 5900 km, and inclination of 70°. Consequently, ABCS spent a significant fraction of its operative life within the inner Van Allen belt, a region of the magnetosphere characterized by high-energy protons and of scientific interest for microsatellite deep space missions [4].

From the beginning of mission analysis, it was clear that ABCS would collect a total ionizing dose (TID) significantly higher than that collected by CubeSats in low Earth orbit (LEO), up to four orders of magnitude more (see Figure 1), resulting in an estimated operative life of less than three days.

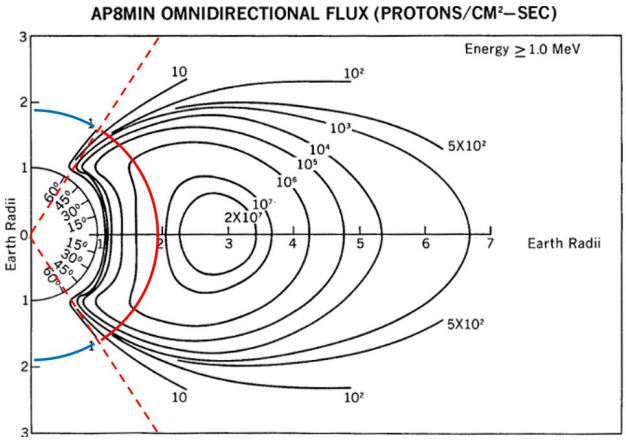

Figure 1. Contour plot of intensity flux for protons [5] and projection of ABCS orbit inside (red) and outside (blue) the inner Van Allen belt.

To ensure that the satellite could reach a stable and known attitude within a sufficiently short time, defined as 24 h from the deployment, it was equipped with an attitude control system. Due to limitations on the electric power budget [6], the selection of a passive magnetic attitude control system (PMACS) was selected for achieving these tasks [7].

A PMACS includes magnets with two distinct behaviours: (1) magnetically hard, named permanent magnets, and (2) magnetically soft, named hysteresis dampers [8]. Both the devices produce a torque as a result of their interaction with the geomagnetic field. In particular, the permanent magnets (1) provide the control torque which aligns the spacecraft toward the direction of the geomagnetic induction vector, whereas the magnetically soft devices (2) generate the damping torque that dissipates the rotational kinetic energy of the satellite and ensures the stability of the attitude motion [9].

PMACS have been extensively used since the beginning of space exploration. Transit-1B, launched in April 1960, was the first spacecraft equipped with magnetic devices, and proved the suitability of PMACS to perform attitude control [10]. In the 1960s and 1970s, PMACS were successfully implemented on ESRO-1A, Azur-1, and Magion, the first satellite by, respectively, ESA, Germany, and Czechoslovakia, and in the EXOS and Injun programs, developed by ISAS and NASA, dedicated to the study of the magnetosphere [11–13]. A detailed review of early satellites equipped with PMACS is provided by Sarychev and Ovchinnikov [14]. More recently, PMACS were succesfully implemented onboard micro- [15–18] and nanosatellites [19,20].

Magnetically soft devices used in PMACS have the shape of elongated rods [8–20], and are therefore called hysteresis rods or bars. A hysteresis rod generates a magnetic dipole moment (almost) parallel to the axis of the rod, and its intensity depends on the magnetic permeability of the rod and its volume. In fact, the magnetic permeability itself depends on the geometry of the rod, and various numerical models have been proposed in the literature to calculate it [21,22].

Due to geometric constraints of ABCS and the nature and intensity of mechanical loads during the launch, the mechanical integration of hysteresis rods to the satellite structure was not possible; therefore, magnetically soft devices in the shape of thin strips, hereafter called hysteresis strips, were used. The effectiveness of hysteresis strips in stabilizing a small satellite was investigated by Fiorillo et al. [23] and Lee et al. [24] by means of numerical analysis, which requires characterizing the hysteresis strips in terms of energy dissipation per cycle and magnetic permeability, quantities that can be extrapolated from the hysteresis loop. Most of the models available in the literature refer to hysteresis rods, the behavior of which can be significantly different from that of the strips [25]. Other models may lack of accuracy because they investigate rods of square cross-section [26], or thin films with thickness lower than $t < 1$ µm [27]. In fact, the literature lacks experimental

data, either from ground tests or flight operations, regarding the hysteresis strips and the related PMACS.

In this research work, we present a mixed numerical–experimental approach to design and characterize a PMACS equipped with permanent magnets and hysteresis strips. The method was successfully applied to design the PMACS of ABCS. The primary goal of this work is to characterize the performance of the PMACS in terms of stabilization time and pointing accuracy.

The magnetic dipole moment generated by each hysteresis strip is determined by two different tests. One test allows for reconstructing the hysteresis loop of the strip when it interacts with a time-varying magnetic field, equivalent to the that experienced by ABCS during its orbital motion, generated by a Helmholtz cage facility. The magnetic permeability and the energy dissipation per cycle are then extracted from the hysteresis loop.

A second test is performed on the engineering unit of ABCS, equivalent to the flight unit and, therefore, including the PMACS. This satellite prototype is mounted to a spherical air-bearing located in the test volume of the Helmholtz cage, and this test setup is used to reproduce the attitude motion in environmental conditions equivalent to the ones of ABCS. The angular rates, collected by a gyroscope integrated to the prototype, together with the known values of the magnetic field and inertial parameters, allow computing the damping torque and from it the magnetic dipole moment. Once the hysteresis strips have been characterized, the number of permanent magnets to be included in the PMACS is determined by numerical analysis, which allows for estimating the pointing accuracy, completing the characterization of the system. The results from laboratory testing are finally validated by analyzing the flight data collected by ABCS.

The paper is organized as follows. The concept design and the theoretical background on passive magnetic attitude control are reported in Section 2. The characterization of the hysteresis strips and of the PMACS stabilization capabilities is performed from experiments described in Section 3. In Section 4, the selection of the number of permanent magnets is determined by using numerical analysis. Final remarks and comments are reported in Section 5.

2. Theoretical Background and Experimental Setup

The 3U ABCS was equipped with a PMACS aimed at ensuring its stabilization toward the geomagnetic field vector (**B**). Noting that $\mathcal{F}_b = \begin{bmatrix} \hat{x}_b & \hat{y}_b & \hat{z}_b \end{bmatrix}$ for the body-fixed reference frame, with its origin in the center of mass of ABCS and the axes orthogonal to the faces of the satellite as in Figure 2, the PMACS was designed to align $\hat{z}_b$ with **B**, ensuring that, for a fraction of ABCS orbit, the four body-mounted solar panels are nearly orthogonal to the direction of the solar radiation.

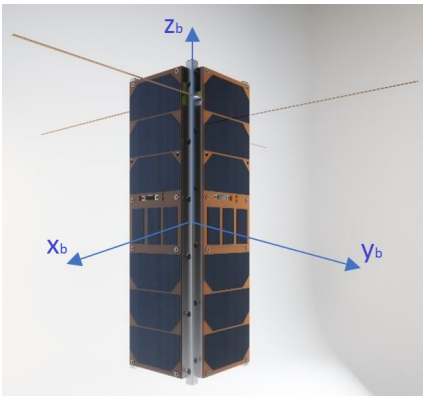

Figure 2. Representation of ABCS and its body-fixed reference frame.

The PMACS includes:

- Four cylindrical neodymium magnets with an outer and inner diameter of 7 and 3.4 mm, respectively, and a height of 11.5 mm, located on the thin edge of one of interface rib (see Figure 3a,b);
- Four hysteresis strips, obtained from a coil of EFI Alloy 79 annealed, with width $w = 9.4$ mm and thickness $t = 0.355$ mm, selected because of the high relative permeability of the material $\mu^{(m)}$ = 461,000, located within the slots of volume $65 \times 10 \times 0.5$ mm^3 realized on each one of the four outer panels (see Figure 3c,d), and fixed by using a space qualified bi-component epoxy resin.

The operating principles of the PMACS and its components are described in the following subsections.

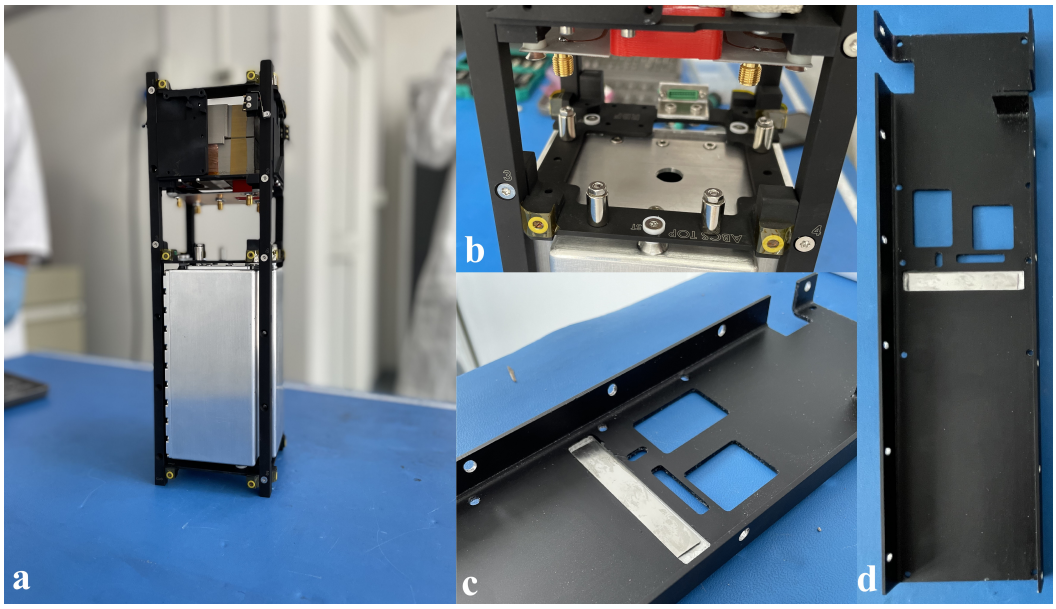

Figure 3. The structure of ABCS (**a**) and the position of the four permanent magnets (**b**) and four hysteresis strips (**c**,**d**) in it.

2.1. Permanent Magnets

The interaction between the magnetic dipole moment **m** generated by a magnet and the geomagnetic field **B** produces a pointing torque according to the following equation [7]

$$\mathbf{T} = \mathbf{m} \times \mathbf{B} \tag{1}$$

For magnets of cylindrical shape, the direction of **m**, indicated as $\hat{m}$, is well approximated by the axis of the magnet; furthermore, for a permanent magnet $m_p = |\mathbf{m}_p|$ is constant, and then Equation (1) can be rearranged as follows,

$$\mathbf{T}_p = m_p \hat{z}_b \times \mathbf{B}, \tag{2}$$

where $\mathbf{T}_p$ is conservative and equal to zero only for $\hat{z}_b \parallel \hat{B}$.

As a consequence of the conservative nature of $\mathbf{T}_p$, the use of permanent magnets alone does not allow us to stabilize the satellite in the desired attitude ($\hat{z}_b \parallel \hat{B}$): the hysteresis strips are introduced for this purpose.

2.2. Hysteresis Dampers

Equation (1) also applies to devices made of magnetically soft materials, such as hysteresis strips. In this case, the evaluation of the magnetic dipole moment $\mathbf{m}_h$ is more

complex, because it depends on the shape and magnetic permeability of the device [7,8]. The evaluation of $\mathbf{m}_h$ is quite simple for hysteresis rods [21] with

$$\mathbf{m}_h = \mu_h V_h H \hat{m}_h, \tag{3}$$

where μ_h and V_h are, respectively, the apparent permeability and the volume of the rod, H is the magnetic field strength in the surrounding of the rod and $\hat{m}_h$ is in the direction of the rod axis of symmetry.

The apparent permeability depends on both the relative permeability of the material $\mu^{(m)}$ and the shape of the rod. A simple expression to calculate μ_h is available for rods with diameter d much smaller than the length l [28]

$$\mu_h = \frac{\mu^m(H)}{1 + N\mu^m(H)}, \tag{4}$$

where

$$N = \left(\frac{4l}{d\sqrt{\pi}} + 2\right)^{-1}. \tag{5}$$

As mentioned in Section 1, geometry constraints led the selection of hysteresis strips instead of rods. Extending Equations (4) and (5) to non-cylindrical magnets is not trivial. Rhodes and Rowlands have proposed a model suitable for square cross-section bars ($w \times w$) [21], which is reported below in the compact form presented by Sato and Ishli [26],

$$\mu_h = k\frac{\mu^m(H)}{1 + N\mu^m(H)} \tag{6}$$

$$N = \left(2\frac{l}{w} + 1\right)^{-1}, \tag{7}$$

where k is a corrective factor which ranges between 0.55 and 0.65.

An equivalent form to the Equation (6) is not available in the literature for hysteresis strips ($t \times w$, $t << w$), and the value of μ_h is either derived from analytical or semiempirical methods [23,25], which put in evidence the nonlinear dependence of μ_h on t/w. In Section 3, two experimental methods are proposed, aimed at characterizing the hysteresis strips in terms of energy dissipated per hysteresis cycle (W_h) and apparent permeability.

2.3. Passive Magnetic Attitude Control

The attitude of ABCS is here described by using the quaternion $\mathbf{q} = [\ \boldsymbol{\epsilon} \quad q_0\ ]^T$, representing the rotation of the body frame $\mathcal{F}_b$, attached to the rigid spacecraft, with respect to an inertial reference frame $\mathcal{F}_i$, here selected as the geocentric inertial frame (GCI). Noting that $\boldsymbol{\omega}$, the angular velocity of $\mathcal{F}_b$ with respect to $\mathcal{F}_i$, the attitude dynamics of the spacecraft equipped with the PMACS can be defined by the following set of ordinary differential equations,

$$\begin{cases} \dot{\boldsymbol{\epsilon}} = \frac{1}{2}(q_0\boldsymbol{\omega} - \boldsymbol{\omega} \times \boldsymbol{\epsilon}) \\ \dot{q}_0 = -\frac{1}{2}\boldsymbol{\epsilon}^T\boldsymbol{\omega} \\ \dot{\boldsymbol{\omega}} = I^{-1}(-\boldsymbol{\omega} \times I\boldsymbol{\omega} + \mathbf{m} \times \mathbf{B_b}) \end{cases}, \tag{8}$$

where $\mathbf{B}_b$ is the geomagnetic field vector projected in the body reference frame [29], and $\mathbf{m}$ is the sum of $\mathbf{m}_p$ and $\mathbf{m}_h$

$$\mathbf{m} = m_h(\hat{x}_b + \hat{y}_b) + m_p\hat{z}_b. \tag{9}$$

It is worth noting here that the hysteresis strips produce a magnetic dipole moment along the $\hat{x}_b$ and $\hat{y}_b$ directions (see Figure 2) by virtue of their location inside ABCS (see Figure 3c,d).

To adequately replicate the effect of the hysteresis strips, the value of m_h shall change according to the hysteresis loop [22],

$$\begin{cases} m_h = \frac{2V_h}{\pi\mu_0} B_s \tan^{-1}[p(B_i/\mu_0 + H_c)] \leftrightarrow \frac{dB_i}{dt} < 0 \\ m_h = \frac{2V_h}{\pi\mu_0} B_s \tan^{-1}[p(B_i/\mu_0 - H_c)] \leftrightarrow \frac{dB_i}{dt} > 0 \end{cases}, \tag{10}$$

with $p = \frac{1}{H_c} \tan\left(\frac{\pi B_r}{2B_i\mu_h}\right)$, where V_h is the volume of the hysteresis strip, B_i is the magnetic field intensity along the ith direction, B_r is the magnetic remanence and B_s is the saturation induction of the strip.

3. Experimental Characterization of the Passive Magnetic Attitude Control System

The apparent permeability μ_h is a key parameter by which to characterize magnetically soft devices and their effect in PMACS because there are no analytical models available in the literature to calculate μ_h for the hysteresis strips (see Section 2.2), and then the parameter shall be determined experimentally.

A simple and effective solution, widely applied for the experimental characterization of hysteresis rods, is represented by the induction method, in which the rod interacts with the periodically changing magnetic field generated by a solenoid, with known geometric and electric characteristics, and whose magnetization is computed indirectly from the current induced to a measurement coil [30]. Plotting the values of magnetization corresponding to each time-varying value of the magnetic field, the magnetic hysteresis loop is obtained and μ_h is calculated from it.

When applied to magnets that are not axisymmetric bodies, the induction method defaults, and an alternate approach shall be followed. An alternate solution, proposed by the authors of this work [6], consists in exciting the hysteresis strip with a time varying magnetic field H, generated by means of a Helmholtz cage in the range corresponding to the geomagnetic field intensity at the orbital altitude of ABCS, and measuring the magnetic flux density B in the surrounding of the hysteresis strip by means of a three-axis magnetometer

$$\mathbf{B} = f(\mu_h)\mu_0\mathbf{H}, \tag{11}$$

where μ_0 is the vacuum permeability. The couple of values (H, B) allows for reconstructing the hysteresis loop of the strip and calculating the corresponding value of μ_h, as detailed in Section 3.2.

A second solution, which allows for validating the above method, is proposed in Section 3.3. Following this different approach, it was possible to evaluate in the laboratory the damping torque introduced on ABCS by the hysteresis strips and extract from it the value of μ_h.

3.1. Helmholtz Cage and Spherical Air-Bearing

To recreate a desired time evolution of the magnetic field in intensity and direction, a Helmholtz cage is used. The facility, represented in Figure 4, can generate a uniform magnetic field in a test volume of $30 \times 30 \times 30$ cm^3 located at the centre of the cage. Each pair of coils can produce a magnetic field in the range $\pm 2 \times 10^{-4}$ T according to the following characteristic curve [31],

$$B = \frac{2\mu_0 NI}{\pi l} \frac{2}{(1+\beta^2)\sqrt{2+\beta^2}}, \tag{12}$$

where I is the current in the coils, $N = 54$ is the number of turns, $l = 1.24$ m is the half-length of the coils and $\beta = 0.5445$ is the distance between the two coils normalized by the half-length. The values of I are determined by the facility control computer as follows:

1. using an orbit propagator, the position $\mathbf{r}(t)$ of the satellite is updated in time;

2. using a model for the geomagnetic field the value $\mathbf{B}_o$ corresponding to $\mathbf{r}(t)$ is calculated, here the International Geomagnetic Reference Field-13 (IGRF) model is used [32]);
3. the actual $\mathbf{B}_g$ in the test volume of the Helmholtz cage is measured from a three-axis magnetometer;
4. the vector $\mathbf{B}_c = \mathbf{B}_o - \mathbf{B}_g$ is calculated and the value of I corresponding to each component of $\mathbf{B}_c$ are computed inverting Equation (12); and
5. a dedicated power supply, actuated by the computer, provides the electric current I to each pair of coils.

The calibration of the three-axis magnetometer and the use of a digital proportional–integral–derivative (PID) controller allow for reproducing the target magnetic field with an accuracy of 10^{-8} T [33].

Figure 4. The Helmholtz cage at the School of Aerospace Engineering "Michele D. Sirinian" Flight Mechanics Laboratory, Sapienza University of Rome.

A spherical air-bearing is located at the center of the test volume. The device includes a support cup, with radius of curvature of 30 cm, which supplies pressurized air from the six holes located in its upper surface. A spherical support with the same radius of curvature is placed on the support cup. When pressurized air is supplied, an air cushion is generated between the two parts, and therefore the spherical support can rotate with negligible friction with respect to the support cup. Satellites up to 12U CubeSats can be integrated to the spherical support to test their attitude motion in an almost frictionless environment, representative of the orbit conditions.

3.2. Experimental Characterization of the Hysteresis Strips

The apparent permeability of the hysteresis strips can be determined after recreating the hysteresis loop for different profiles of the time-varying magnetic field. The following method, proposed by the authors, was successfully applied to characterize the hysteresis strips used for ABCS [6]:

1. A desired profile of the magnetic field (H) is recreated inside the Helmholtz cage. Two cases were examined for ABCS, with limit values of the magnetic field compatible with the ones in the operative orbit:
   (a) Triangular variation between $\pm 8 \times 10^{-3}$ A/m;
   (b) Sinusoidal variation between $\pm 8 \times 10^{-3}$ A/m;
2. The magnetic flux density on the surface of the hysteresis strip $\mathbf{B}_h$ is measured using a magnetic field probe operating at a sampling frequency of 10 Hz; and

3. The hysteresis loop (B_h, H) is reconstructed, the value of μ_h is calculated from Equation (11).

The results of the characterization for the hysteresis strips of ABCS are described hereafter. Because the hysteresis strips are aimed at damping the attitude motion of the spacecraft along the $\hat{x}_b$ and $\hat{y}_b$ directions, the value of $\mathbf{B}_h$ along the longitudinal axis of the strip (see Figure 2) is examined in detail. Each test case (a–b) was repeated 10 times, producing 20 different hysteresis loops, one of which is reported in Figure 5. It can be observed that the hysteresis strips never saturate in the ABCS operative conditions [34].

Recalling now that the hysteresis loop area represents the energy dissipation per cycle, the area for each loop was calculated and averaged, obtaining a mean $W_h = 6.28 \times 10^{-8}$ J. The result was compared to the one obtained in equivalent conditions from the semiempirical method by Farrahi and Sanz-Andrés [25], resulting in a difference lower than the 10%.

The apparent permeability of the hysteresis strips was calculated from Equation (11), resulting in a mean $\mu_h = 10.6$ and a maximum $\mu_h^{max} = 22.4$. The reader will notice that the value of the apparent permeability determined from the experimental campaign is rather far from the one that can be obtained from Equations (4) and (5) or Equations (6) and (7) given the known relative permeability of the material $\mu^{(m)}$ = 461,000 and the length and thickness of the strip, respectively equal to $l = 65$ mm and $t = 0.355$ mm.

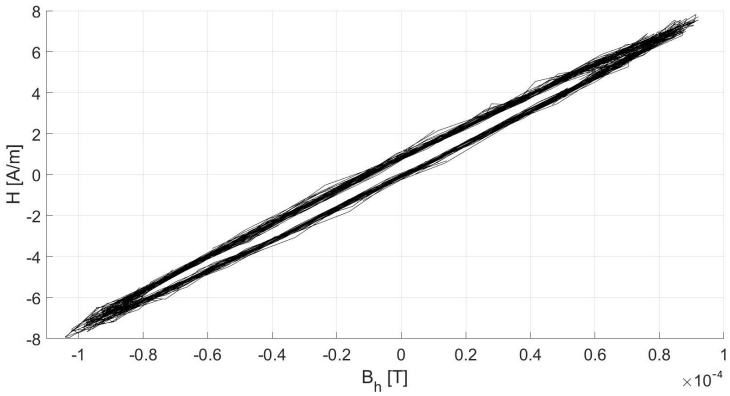

Figure 5. A hysteresis loop obtained for the strips during the experimental campaign.

3.3. Experimental Evaluation of the Stabilization Performance

The apparent permeability can be determined from another experimental approach based on the known values of the magnetic field H, generated by the Helmholtz cage, and of the angular velocity $\boldsymbol{\omega}$ of a representative testbed equipped with the PMACS and integrated to the air-bearing, measured by using a gyroscope.

The method consists of the following steps:

1. The testbed, equipped with the PMACS, is integrated to the spherical support and placed inside the Helmholtz cage with known attitude. For the test case examined hereafter, the testbed is the engineering unit of ABCS, that was placed in the Helmholtz cage with axis x_b parallel to the local vertical direction, as shown in Figure 6.
2. The testbed is spun at a known angular rate. ABCS was spun at an angular rate of $\omega_x = 2.5°/\text{s}$, representative of the deployment conditions.
3. The angular velocity ($\boldsymbol{\omega}$) and the magnetic field ($\mathbf{B}_b$) are measured by using calibrated three-axis gyroscope and magnetometer fixed to the testbed. For ABCS, a datalogger operating at a sampling frequency of 100 Hz was used. The angular acceleration is computed from the measured data.

4. The last one of Equations (8) is used to determine **m**, given the known tensor of inertia for the testbed. In particular, for ABCS the component $m_h \hat{x}_b$ was computed based on the following tensor of inertia evaluated in $\mathcal{F}_b$,

$$\mathbf{I}_a = \begin{bmatrix} 0.50941 & 0.00043 & 0.00034 \\ 0.00044 & 0.51007 & 0.00755 \\ 0.00034 & 0.00755 & 0.10231 \end{bmatrix} \text{kg} \cdot \text{m}^2.$$

5. Finally, μ_h is computed from Equation (3).

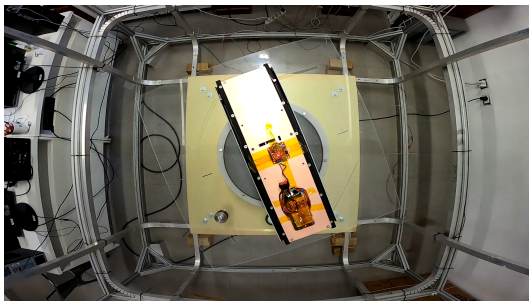

Figure 6. The engineering unit of ABCS integrated to the facility and diagnostic devices (on top).

As mentioned above, the method was applied to characterize the PMACS integrated to ABCS. Limitations on the pressurized air-distribution system did not allow for performing tests longer than 15 min, a time significantly shorter than that desired for the stabilization of the satellite, which can be as high as 24 h. In order to reduce the time required to have an evidence of the damping effect on the testbed, the magnetic field generated by the Helmholtz cage during the tests had the same time behavior of that corresponding to the circular orbit of ABCS, with semimajor axis of 5900 km and inclination of 70°, but its magnitude was scaled up by a factor of 10.

Figure 7 shows the angular rate ω_x measured by the gyroscope (red) and its interpolation (black). Following the sequence of operations (1–5), it was determined that a mean angular deceleration $\dot{\omega}_x = 2.29 \times 10^{-5}$ °/s^2, corresponding to a magnetic dipole moment $m_{h,x} = 8.88 \times 10^{-4}$ Am^2 and an apparent permeability $\mu_h^{(exp)} = 11.2$ for each hysteresis strip.

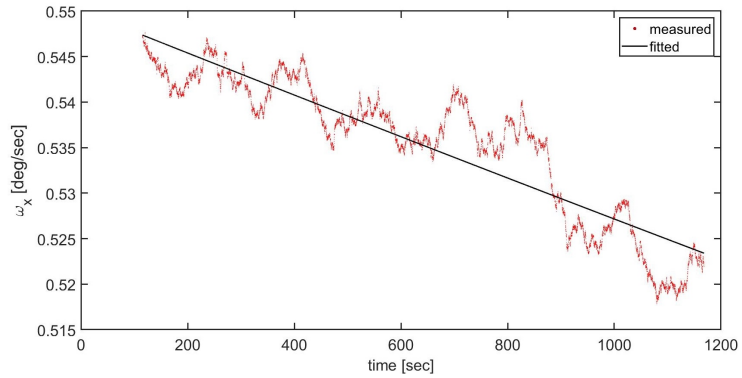

Figure 7. Measured (red) and interpolated (black) angular velocity during the PMACS characterization test.

It shall be observed that for higher angular rates the number of hysteresis cycles for unit of time increases. Therefore, assuming that the average energy dissipation per loop is constant $W_h = 6.28 \times 10^{-8}$ J, the higher the angular rates, the higher the energy dissipated by the PMACS and the mangitude of the deceleration.

The time required for the detumbling of a satellite with tensor of inertia **I** and angular velocity $\boldsymbol{\omega}_0$ at the deployment can be determined from the mean deceleration $\bar{\dot{\omega}}$

$$t_d^{(exp)} = \frac{\boldsymbol{\omega}_0}{\bar{\dot{\omega}}}. \tag{13}$$

The mean deceleration computed for ABCS was $\bar{\dot{\omega}} = 2.3 \times 10^{-5}\ ^\circ/\mathrm{s}^2$ (recall that the data used to calculate $\bar{\dot{\omega}}$ was collected during a test campaign in which the magnetic field intensity was 10 times higher than the one experienced during the ABCS mission). It follows that the PMACS can perform the detumbling of the satellite in the prescribed 24 h for ω_0 lower than $2\ ^\circ/\mathrm{s}$. This result matches well with the one obtained by applying the expression suggested by Farrahi and Sanz-Andrés to determine the detumbling time [25]

$$t_d = \frac{\pi^2 I_{xx}}{180 W_h} \tag{14}$$

where I_{xx} is the first component of the tensor of inertia, reported below for ABCS:

$$\mathbf{I} = \begin{bmatrix} 0.0495 & 0.0000 & 0.0010 \\ 0.0000 & 0.0492 & 0.0001 \\ 0.0010 & 0.0001 & 0.0102 \end{bmatrix} \mathrm{kg} \cdot \mathrm{m}^2. \tag{15}$$

Comparing the results obtained from Equations (13) and (14) by using the data reported for ABCS, it can be observed that the error between the two is about 1%.

For ABCS, the angular rates at the deployment were expected to range within $\pm 2.5\ ^\circ/\mathrm{s}$, and then the stabilization performance of the PMACS would be considered satisfactory because it would be capable of reducing the rates by one order of magnitude on the first day of the mission.

4. Numerical Analysis and Validation of the Passive Magnetic Attitude Control System

Once verified, the stability performance of the PMACS, the number of permanent magnets required to produce the desired pointing accuracy was determined from numerical analysis.

The attitude motion of ABCS was simulated by modeling the spacecraft as a rigid body (see Section 2.3) on which only the magnetic torque acts, expressed by Equation (1) and Equation (9). In fact, the major disturbance torques which shall be taken into account in LEO, due to the aerodynamic drag and the gravity gradient, are negligible for the ABCS mission by virtue of the high orbital altitude of the spacecraft ($h = 5900$ km). The torque induced by the solar radiation pressure was neglected because of the geometry of the 3U CubeSat ABCS, characterized by a small cross-section and a maximum displacement between the center of mass and the center of pressure never exceeding 49.5 mm.

The results from numerical analysis allowed evaluating the performance of the PMACS also in terms of pointing accuracy. At the end of this section, the numerical results are compared to the experimental ones obtained by processing the data collected by the onboard three-axis magnetometer and gyroscope during the first orbits of ABCS.

4.1. Numerical Analysis

The attitude dynamics of ABCS was simulated by integrating the set of nonlinear equations of motion (8). The components of the quaternion and the angular rates at the initial time of the simulation, corresponding to the deployment, were selected randomly, with the rates limited in the range $\pm 2.5\ ^\circ/\mathrm{s}$.

Three test cases were examined, differing by the number of permanent magnets equal to, respectively, 1, 2 and 4, the maximum number which can fit onboard ABCS. Each permanent magnet generates a magnetic dipole moment equal to 0.3095 Am^2 along the axis of symmetry, whereas the component in the radial direction is neglected. The magnetic dipole moment generated by each one of the four hysteresis strips is calculated from

Equation (10) by using the parameters reported in Table 1, obtained from the experimental characterization campaign and from the datasheet of the material used for the strips. The geomagnetic field was modeled by using the 12th-generation IGRF model [32].

Table 1. Parameters of the hysteresis strips.

Parameter	Symbol	Value
Apparent permeability	μ_h	10.6
Coercivity	H_c	0.4487 A/m
Remanence	B_r	0.3610 T
Saturation induction	B_s	0.6800 T

Figures 8–10 show the misalignment error δ_b, namely the angle between the axis $\hat{z}_b$ and $\mathbf{B}_b$, for the three test cases with, respectively, 1, 2, and 4 permanent magnets. It can be observed that the higher the number of permanent magnets, the shorter the time required for δ_b to decrease within the error band $\pm 10°$. As shown in Figure 10, a total of 4 permanent magnets are required to reach the pointing performance within the target time of 24 h from the deyploment, corresponding to 6 orbits.

The numerical analysis also allows for further evaluation of the damping effect introduced by the four hysteresis strips, which is here measured in terms of the rotational kinetic energy, defined as follows:

$$K = \frac{1}{2}\boldsymbol{\omega}^T \mathbf{I}\boldsymbol{\omega}. \tag{16}$$

The time behavior of K, for the PMACS equipped with 4 permanent magnets, is reported in Figure 11, showing that the quantity decreases, at the rate inferred from the test discussed in Section 3.

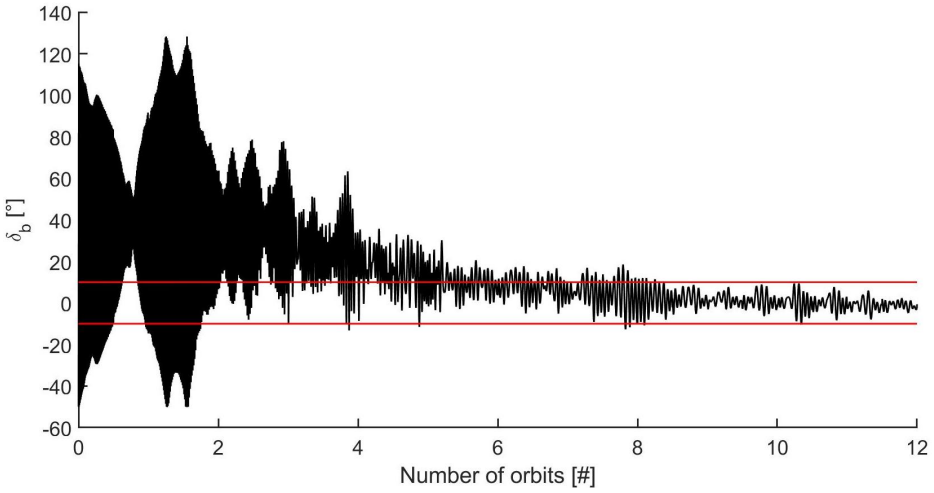

Figure 8. Misalignment error between $\hat{z}_b$ and $\mathbf{B}_b$ for PMACS with 1 permanent magnet.

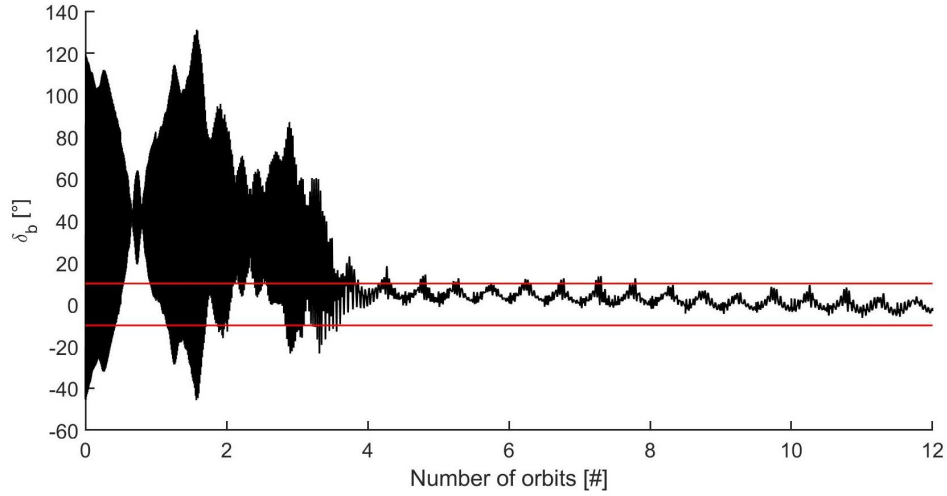

Figure 9. Misalignment error between $\hat{z}_b$ and $\mathbf{B}_b$ for PMACS with 2 permanent magnets.

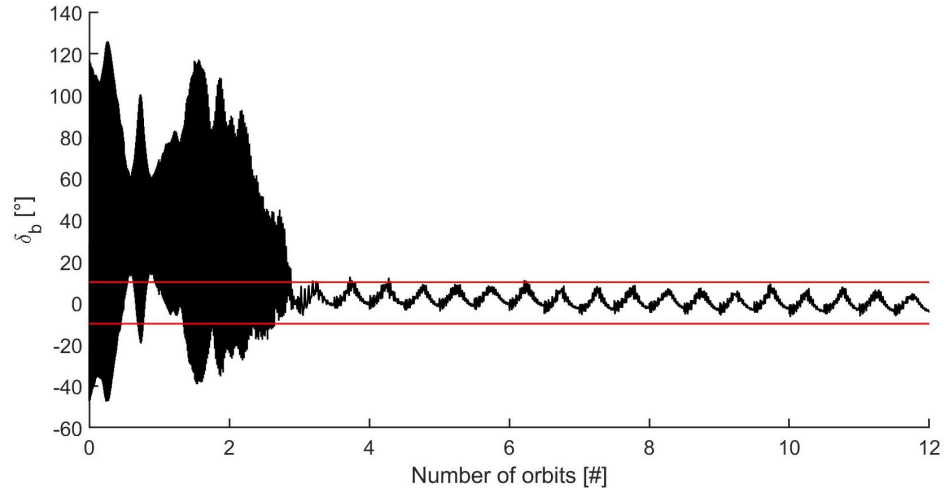

Figure 10. Misalignment error between $\hat{z}_b$ and $\mathbf{B}_b$ for PMACS with 4 permanent magnets.

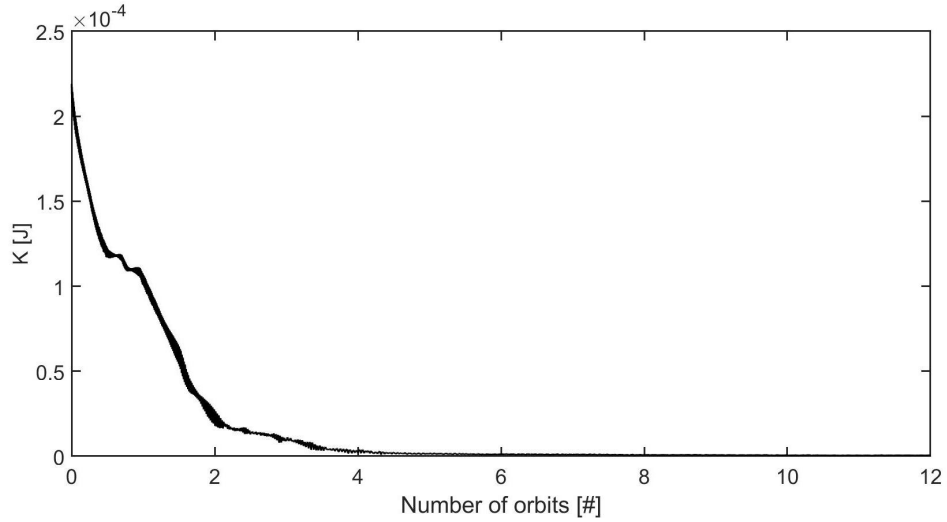

Figure 11. Time evolution of the rotational kinetic energy of ABCS with 4 permanent magnets.

4.2. Analysis of Flight Data

The results from the simulations were finally compared with the flight data collected during the first day of operations after the deployment of ABCS from Vega C, on 13 July 2022. ABCS was equipped with a three-axis gyroscope and a three-axis magnetometer, both integrated to the satellite on-board computer [35,36]. The data processed here were downloaded from the ground station of the School of Aerospace Engineering of Rome and from other amateur radio stations at the support of the mission. For each data package received, the measurements from both of the sensors were processed by using a low-pass filter with cut-off frequency of 1 Hz.

The gyroscope data was used to compute the rotational kinetic energy of ABCS, shown in Figure 12 where the marker indicate the measured values and the dashed line, connecting them, was added to have a clearer view of the behavior of K over time. The reader will notice that the damping is faster in certain time intervals. This occurs when the satellite has latitude in the band $\pm 25^\circ$ and is outside the Earth shadow. Although the angular rates at the deployment were higher than expected, the measurements indicate that the PMACS performed well in stabilizing the satellite.

Data from the magnetometer was used to calculate the misalignment error, whose values are shown in Figure 13. Flight data indicates that δ_b enters the $\pm 10^\circ$ error band after two orbits; despite the fact that it is not possible to exclude the δ_b evolving outside the error band between two consecutive measurements, it is evidence that the PMACS tended to control the attitude of ABCS such that $\hat{z}_b$ was pointing toward the geomagnetic field induction vector.

It is worth noting, in conclusion of this study, that differences from the numerical analysis and the flight data can also be due to limits of the IGRF model, which is technically designed for altitudes below 600 km, although it is often used for higher orbits, in representing the geomagnetic field in the inner Van Allen Belt.

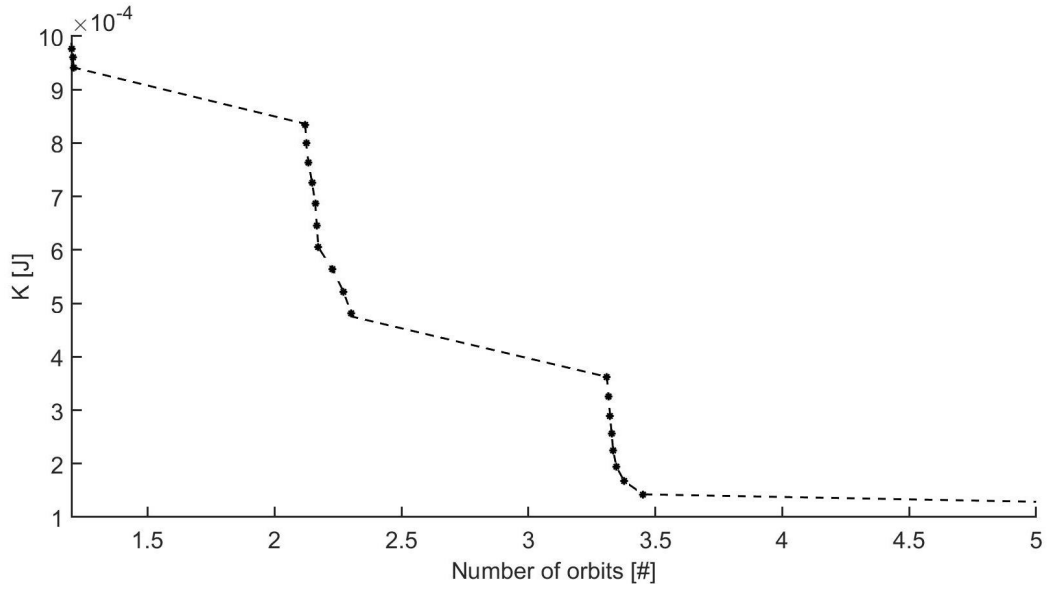

Figure 12. Time evolution of the rotational kinetic energy during the first orbits of ABCS: measured (✻) and fitted (dashed line) data.

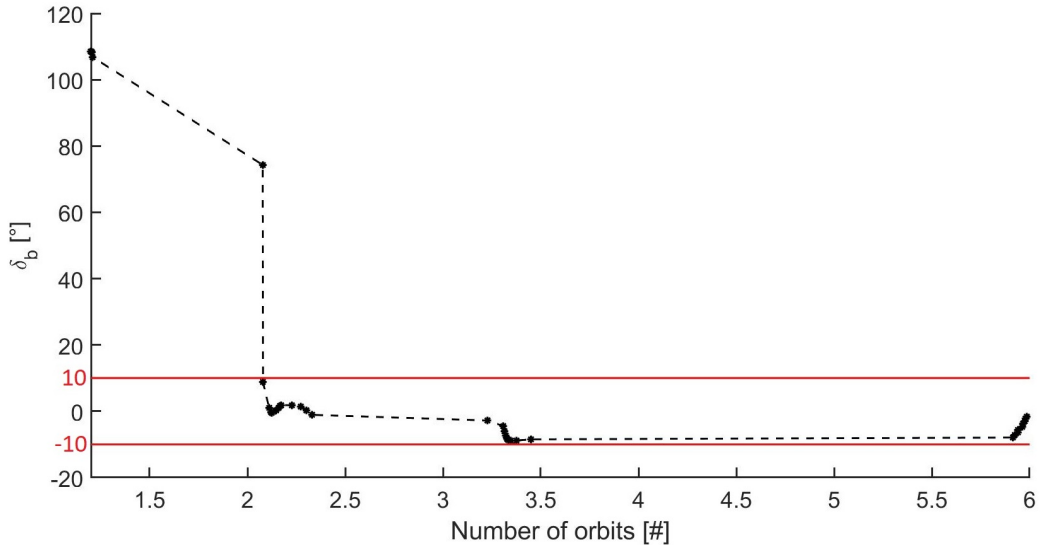

Figure 13. Misalignment error between $\hat{z}_b$ and $\mathbf{B}_b$ during the first orbits of ABCS: measured (✳) and fitted (dashed line) data.

5. Conclusions

This paper presents two experimental methods aimed at characterizing (i) the apparent magnetic permeability (μ_h) and energy dissipation per hysteresis cycle (W_h) of soft magnets in the shape of thin strips and (ii) the damping performance of a PMACS equipped with the mentioned hysteresis strips. The methods were applied to design the PMACS for the 3U ABCS.

The method (i) allowed for determining $\mu_h = 10.6$ and $W_h = 6.28 \times 10^{-8}$ J for ABCS, confirming that models used for hysteresis dampers in the shape of elongated rods are not adequate for hysteresis strips, and they can introduce a large error, which was quantified in the 200%.

The PMACS, including four hysteresis strips of volume $65 \times 9.4 \times 0.355$ mm^3, was integrated to the engineering unit of ABCS and a test campaign was performed to evaluate method (ii). The use of air-bearing and Helmholtz cage facilities allowed for recreating an environment almost equivalent, for the sake of the test, to the one experienced by the spacecraft in orbit. By measuring the time evolution of the angular rates, it was possible to estimate the damping torque and consequently the apparent permeability of the strips, resulting in $\mu_h^{(exp)} = 11.2$.

The two values of the magnetic permeability of the hysteresis strips differs by the 5.5%, showing a good matching between methods (i) and (ii). Once defined, the model for the hysteresis strip, numerical simulation were performed to select the number of permanent magnets which ensures the desired pointing accuracy for ABCS, within the target time of 24 h from the deployment. The analysis indicated that a total of four permanent magnets with magnetic dipole moment of $m_p = 0.3095$ Am^2 were necessary.

The performance of the PMACS designed for ABCS, and consequently the effectiveness of methods (i) and (ii), was finally examined based on the flight data received from the spacecraft during the first day after deployment in orbit from Vega C, on 13 July 2022. The analysis of flight data indicated that the rotational kinetic energy of ABCS decreased, as expected, by one order of magnitude in less than 24 h and that, in the meantime, the angle between the axis $\hat{z}_b$ and the geomagnetic field induction vector **B** has reduced to less than 10°.

Author Contributions: Conceptualization, S.C.; methodology, S.C., A.N., S.S.G.M. and L.I.; software, S.S.G.M., T.B.d.A. and N.M.D.; validation, S.C., A.N. and L.S.; formal analysis, S.S.G.M.; investigation, S.C., A.N., S.S.G.M., L.I., T.B.d.A., N.M.D., L.S., G.I., S.P. and J.R.B; resources, S.C., A.N. and L.I.; data curation, S.C. and N.M.D.; writing—original draft preparation, S.C.; writing—review and editing, A.N., S.S.G.M., G.I., S.P. and J.R.B; visualization, L.I.; supervision, S.C., A.N., G.I. and S.P.; project

administration, A.N., S.P. and J.R.B.; funding acquisition, A.N. and J.R.B. All authors have read and agreed to the published version of the manuscript.

Funding: Agreement 2019-30-HH.0 between the Italian Space Agency and the National Institute for Astrophysics.

Conflicts of Interest: The authors declare no conflict of interest.

References

1. Iannascoli, L.; Nascetti, A.; Carletta, S.; Schirone, L.; Meneghin, A.; Brucato, J.R.; Paglialunga, D.; Poggiali, G.; Pirrotta, S.; Impresario, G.; et al. AstroBio CubeSat: Enabling technologies for astrobiology research in space. In Proceedings of the 71st International Astronautical Congress—The CyberSpace Edition, Virtual Online, 12–14 October 2020; p. x60795.
2. Meneghin, A.; Brucato, J.R.; Paglialunga, D.; Nascetti, A.; Fiacco, G.; Pirrotta, S.; Odogoudra, N.; Carletta, S.; Schirone, L.; Granello, P.; et al. AstroBio CubeSat: A nanosatellite for astrobiology experiments in space. *Adv. Astronaut. Sci.* **2020**, *173*, 197–205.
3. Paglialunga, D.; Iannascoli, L.; Calabria, D.; Trozzi, I.; Marchegiani, E.; Zangheri, M.; Guardigli, M.; Mirasoli, M.; Brucato, J.R.; Meneghin, A.; et al. AstroBio CubeSat: On-Ground Validation of Lab-on-Chip Based Astrobiology Experiments. *Lect. Notes Electr. Eng.* **2023**, *918*, 14–20.
4. Graziani, F.; Sparvieri, N.; Carletta, S. A low-cost earth-moon-mars mission using a microsatellite platform. In Proceedings of the 71st International Astronautical Congress (IAC), Virtual Online, 12–14 October 2020; p. x61563.
5. Sqwyer, D.M.; Vette, J.J. *Ap-8 Trapped Proton Environment for Solar Maximum and Solar Minimum*; NASA-TM-X–72605; National Aeronautics and Space Administration: Greenbelt, MD, USA, 1976.
6. Carletta, S.; GosikereMatadha, S.S.; Ramesh, S.V.; Iannascoli, L.; Paglialunga, D.; Nascetti, A.; Schirone, L. Design and experimental characterization of the passive magnetic attitude control system for the 3U AstroBio CubeSat. In Proceedings of the 72nd International Astronautical Congress (IAC), Dubai, United Arab Emirates, 12–14 October 2020; p. x64701.
7. Wertz J.R. *Spacecraft Attitude Determination and Control*; Springer: Dordrecht, The Netherlands, 1978.
8. Bozorth, R.M. *Ferromagnetism*; Van Nostrand: New York, NY, USA, 1951.
9. Ismailova, A.; Zhilisbayeva, K. Passive Magnetic Stabilization of the Rotational Motion of the Satellite in its Inclined Orbit. *Appl. Math. Sci.* **2015**, *9*, 791–802. [CrossRef]
10. Danchik, J.R. An Overview of Transit Development. *Johns Hopkins Apl Tech. Dig.* **1998**, *19*, 18–26.
11. Kummer, H. Satellite Flight Dynamics Data-Handling Systems. *ESA Bull.* **1976**, *7*, 26–31.
12. Ninomiya, K.; Takezawa, S. Digital simulation of the magnetic attitude stabilization for scientific satellite EXOS-A. In Proceedings of the International Symposium on Space Technology and Science, Tokyo, Japan, 30 June–4 July 1975.
13. O'Brien, B.J. High-Latitude Geophysical Studies with Satellite Injun-3 part 1: Description of the satellite. *J. Geophys. Res.* **1964**, *69*, 1–12. [CrossRef]
14. Sarychev, V.A.; Ovchinnikov, M.Y. Magnetic Attitude Control Systems for Earth's Satellites. *Itogi Nauki Tekh. Ser. Issled. Kosm. Prostr.* **1985**, *23*.
15. Ovchinnikov, M.Y. Methods to obtain the principal parameters of simple attitude control systems for small satellites. *Acta Astronaut.* **1998**, *43*, 597–605. [CrossRef]
16. Santoni, F.; Zelli, M. Passive magnetic attitude stabilization of the UNISAT-4 microsatellite. *Acta Astronaut.* **2009**, *65*, 792–803. [CrossRef]
17. Battagliere, M.L.; Santoni, F.; Piergentili, F.; Ovchinnikov, M.; Graziani, F. Passive magnetic attitude stabilization system of the EduSAT microsatellite. *Proc. Inst. Mech. Eng. Part G J. Aerosp. Eng.* **2010**, 224, 1097–1106. [CrossRef]
18. Battistini, S.; Cappelletti, C.; Graziani, F. Results of the attitude reconstruction for the UniSat-6 microsatellite using in-orbit data. *Acta Astronaut.* **2016**, *127*, 87–94. [CrossRef]
19. Marcelino, G.M.; Filho, E.M.; Martinez, S.V.; Seman, L.O.; Bezerra, E.A. In-orbit preliminary results from the open-source educational nanosatellite FloripaSat-I. *Acta Astronaut.* **2021**, *188*, 64–80. [CrossRef]
20. Ovchinnikov, M.Y.; Ilyin, A.A.; Kupriynova, N.V.; Penkov, V.I.; Selivanov, A.S. Attitude dynamics of the first Russian nanosatellite TNS-0. *Acta Astronaut.* **2007**, *61*, 277–285. [CrossRef]
21. Rhodes, P.; Rowlands, G. Demagnetising energies of uniformly magnetized rectangular blocks. *Proc. Leeds Philos. Lit. Soc. Collect.* **1954**, *6*, 191–210.
22. Flatley, T.W.; Henretty, D.A. A Magnetic Hysteresis Model. In Proceedings of the Flight Mechanics Estimation Theory Symposium 1995, Greenbelt, MD, USA, 16–18 May 1995; pp. 405–416.
23. Fiorillo, F.; Santoni, F.; Ferrara, E.; Battagliere, M.L.; Bottauscio, O.; Graziani, F. Soft Magnets for Passive Attitude Stabilization of Small Satellites. *IEEE Trans. Magn.* **2010**, *46*, 670–673. [CrossRef]
24. Lee, D.; Springmann, J.C.; Spangelo, S.C.; Cutler, J.W. Satellite Dynamics Simulator Development Using Lie Group Variational Integrator. In Proceedings of the AIAA Modeling and Simulation Technologies Conference, Portland, OR, USA, 8–11 August 2011.
25. Farrahi, A.; Sanz-Andrés, A. Efficiency of Hysteresis Rods in Small Spacecraft Attitude Stabilization. *Sci. World J.* **2013**, *2013*, 459573. [CrossRef] [PubMed]
26. Sato, M.; Ishli, Y. Simple and approximate expressions of demagnetizing factors of uniformly magnetized rectangular rod and cylinder. *J. Appl. Phys.* **1989**, *66*, 983–985. [CrossRef]

27. Kern, P.R.; da Silva, O.E.; de Siqueira, J.V.; Della Pace, R.D.; Rigue, J.N.; Carara, M. A study on the thickness dependence of static and dynamic magnetic properties of Ni81Fe19 thin films. *J. Magn. Magn. Mater.* **2016**, *419*, 456–463. [CrossRef]
28. Gerhardt, D.T.; Palo, S.E. Passive Magnetic Attitude Control for CubeSat Spacecraft. In Proceedings of the 24th Annual AIAA/USU Conference on Small Satellites, Logan, UT, USA, 9–12 August 2010.
29. de Ruiter, A.H.; Damaren, C.; Forbes, J.R. *Spacecraft Dynamics and Control: An Introduction*; John Wiley & Sons. Ltd.: Chichester, UK, 2013.
30. Ivanov, D.S.; Ovchinnikov, M.Y.; Pen'kov, V.I. Laboratory Study of Magnetic Properties of Hysteresis Rods for Attitude Control Systems of Minisatellites. *J. Comput. Syst. Sci. Int.* **2013**, *52*, 145–164. [CrossRef]
31. Farissi, M.S.; Carletta, S.; Nascetti, A. Design and hardware-in-the-loop test of an active magnetic detumbling and pointing control based only on three-axis magnetometer data. In Proceedings of the 70th International Astronautical Congress (IAC), Washington, DC, USA, 21–25 October 2019.
32. Thébault, E.; Finlay, C.C.; Zvereva, T. International Geomagnetic Reference Field: The 12th generation. *Earth Planets Space* **2015**, *67*, 79. [CrossRef]
33. Farissi, M.S.; Carletta, S.; Nascetti, A.; Teofilatto, P. Implementation and hardware-in-the-loop simulation of a magnetic detumbling and pointing control based on three-axis magnetometer data. *Aerospace* **2019**, *6*, 133. [CrossRef]
34. Sung, H.; Rudowicz, C. A closer look at the hysteresis loop for ferromagnets—A survey of misconceptions and misinterpretations in textbooks. *arXiv* **2002**, arXiv:cond-mat/0210657.
35. Carletta, S.; Teofilatto, P. Design and Numerical Validation of an Algorithm for the Detumbling and Angular Rate Determination of a CubeSat Using Only Three-Axis Magnetometer Data. *Int. J. Aerosp. Eng.* **2018**, *2018*, 9768475. [CrossRef]
36. Carletta, S.; Teofilatto, P.; Farissi, M.S. A Magnetometer-Only Attitude Determination Strategy for Small Satellites: Design of the Algorithm and Hardware-in-the-Loop Testing. *Aerospace* **2020**, *7*, 3. [CrossRef]